Spectrochimica Acta Part A: Molecular and Biomolecular Spectroscopy 359 (2026) 127926

Contents lists available at ScienceDirect

Spectrochimica Acta Part A:
Molecular and Biomolecular Spectroscopy

journal homepage: www.journals.elsevier.com/spectrochimica-acta-part-a-molecular-and-biomolecular-spectroscopy

Photobleaching-assisted extraction of Raman spectral features from fluorescence-enhanced background variation

Yusuke Shiozaki [a,b,*], Katsumasa Fujita [a,c,*]

[a] Department of Applied Physics, The University of Osaka, 2-1 Yamadaoka, Suita, Osaka 565-0871, Japan
[b] Nanophoton - a Bruker company, 3-1-7, Semba-Nishi, Minoh, Osaka 562-0036, Japan
[c] Institute for Open and Transdisciplinary Research Initiatives, The University of Osaka, 2-1 Yamadaoka, Suita, Osaka 565-0871, Japan

HIGHLIGHTS

- Photobleaching during repeated spectral acquisition enables spectral extraction.
- Instrument-derived spectral variations are suppressed in the extracted Raman spectrum.
- No hardware modifications are required.
- Compatible with conventional Raman instruments.

GRAPHICAL ABSTRACT

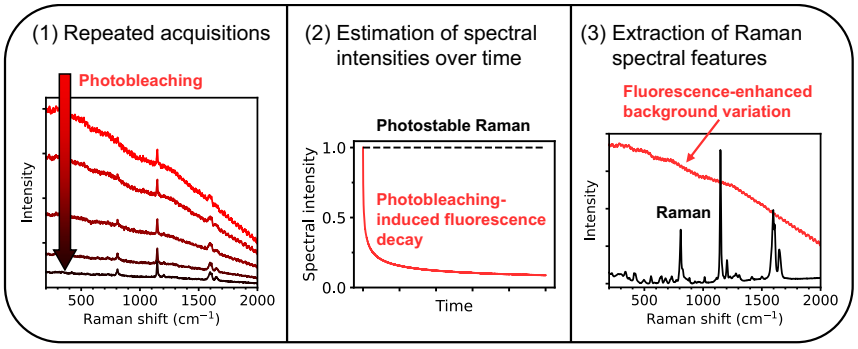

ARTICLE INFO

Keywords:
Spectral feature extraction
Raman spectroscopy
Fluorescence
Photobleaching
Instrument-derived spectral variations

ABSTRACT

We present a photobleaching-assisted method for extracting Raman spectra from fluorescence-dominated signals without hardware modifications. This method involves sequential spectral acquisitions during the photobleaching process and applies a least-squares-based decomposition algorithm to isolate the photostable Raman components from the decaying fluorescence background. This procedure reduces the instrument-derived spectral variations that arise with increasing background intensity, thereby improving the detectability of weak and overlapping Raman bands. The prerequisite conditions of the method are that the shapes of both the observed Raman and fluorescence spectra remain largely unchanged during measurement and that their spectral coefficients can be reasonably estimated from the measurement conditions or measured data. Both proof-of-concept simulations using simulated data and experiments with polystyrene-based fluorescent beads demonstrated that the proposed method can extract Raman spectra by mitigating instrument-derived spectral variations. The application of the proposed method to a highly fluorescent polymer using both 532 and 785 nm excitation wavelengths demonstrates its capability to extract Raman spectral features across different optical configurations. This method broadens the application of Raman measurements under a fluorescence background and provides an additional strategy to enhance existing approaches.

* Corresponding authors at: Department of Applied Physics, The University of Osaka, 2-1 Yamadaoka, Suita, Osaka 565-0871, Japan.
E-mail addresses: shiozaki@ap.eng.osaka-u.ac.jp (Y. Shiozaki), fujita@ap.eng.osaka-u.ac.jp (K. Fujita).

https://doi.org/10.1016/j.saa.2026.127926
Received 10 December 2025; Received in revised form 10 April 2026; Accepted 13 April 2026
Available online 19 April 2026

1. Introduction

In Raman spectroscopy, sample fluorescence adds a background signal and introduces instrument-derived spectral variations, which complicate the interpretation of Raman spectra. Spectral variations include effects such as filter ripple, pixel-to-pixel sensitivity variations in the charge-coupled device (CCD), and etaloning. These effects become prominent when the baseline is elevated by fluorescence [1,2], as they increase proportionally with signal intensity. Unlike random noise, such as shot noise or readout noise, these spectral variations cannot be reduced by averaging.

Fluorescence-removal techniques can be used to eliminate instrument-derived spectral variations associated with fluorescence, thereby facilitating Raman spectral extraction. One such method is shifted excitation Raman difference spectroscopy (SERDS), in which fluorescence is removed by differencing spectra measured at slightly shifted excitation wavelengths, followed by the reconstruction of the Raman spectrum [3]. In the resulting difference spectra, fluorescence and instrument-derived variations are effectively eliminated [4–6]. This approach has been used to extract Raman spectra in the presence of strong fluorescence [5–14].

Herein, we propose a method for extracting Raman spectra with reduced instrument-derived spectral variations by using photobleaching-induced temporal background changes during continuous laser irradiation. To date, photobleaching has been used as a preprocessing step to suppress fluorescence [15–26] rather than to explicitly extract Raman spectra from fluorescence spectral components. Consequently, residual fluorescence background and instrument-derived spectral variations often remain. The present study addresses this limitation by explicitly modeling the temporal intensity changes of fluorescence and separating them from the photostable Raman signal to remove the background, similar to the effect achieved by SERDS. Consequently, the spectral variations associated with fluorescence can be eliminated, allowing an accurate estimation of the Raman spectra. This method requires simple repeated acquisition of spectra without additional hardware beyond a typical Raman spectrophotometer, making it compatible with commercially available systems.

In this paper, we first introduce the principles of the proposed method, followed by proof-of-concept simulations using simulated data and experiments using polystyrene-based fluorescent beads. Next, we demonstrate the application of the proposed method to a highly fluorescent polymer using 532 and 785 nm excitation wavelengths. Finally, the effectiveness and limitations of the proposed method are discussed.

2. Principle

In principle, decomposing a spectrum into two components requires at least two spectra with different component ratios [27,28]. Photobleaching naturally provides an opportunity to acquire such spectra, because the fluorescence component decays over time, whereas the Raman component remains relatively stable. However, under fluorescence-rich conditions, the use of only two spectra often results in an insufficient signal-to-noise ratio (SNR), leading to unreliable decomposition. Therefore, acquiring multiple spectra at different stages of photobleaching provides a wider range of component ratios and facilitates a more robust estimation of the Raman spectrum.

The mathematical model used in the proposed method is presented here. Each measured spectrum is regarded as a linear combination of the photostable Raman spectrum $\boldsymbol{s}_R$ and the fluorescence spectrum $\boldsymbol{s}_F$. The fluorescence intensity decreases with photobleaching, whereas the spectral shape remains unchanged. Accordingly, the i-th spectrum $\boldsymbol{d}_i$ acquired during photobleaching is expressed as.

$$\boldsymbol{d}_i \approx c_{F(i)}\boldsymbol{s}_F + c_{R(i)}\boldsymbol{s}_R \tag{1}$$

where $c_{F(i)}$ and $c_{R(i)}$ denote the fluorescence and Raman intensity coefficient of the i-th spectrum, respectively. The prerequisite conditions for this method are that the shapes of both the observed Raman and fluorescence spectra remain largely unchanged during measurement, and their spectral coefficients can be estimated from the measurement conditions or measured data. Collecting n spectra yields the data matrix $= [\boldsymbol{d}_1, \boldsymbol{d}_2, \cdots, \boldsymbol{d}_n]^T$, which is written as:

$$\boldsymbol{D} \approx \boldsymbol{C}\,\boldsymbol{S}^T \tag{2}$$

where $\boldsymbol{C} = [\boldsymbol{c}_F, \boldsymbol{c}_R]$ and $\boldsymbol{S} = [\boldsymbol{s}_F, \boldsymbol{s}_R]$ contain the intensity coefficients and spectral components, respectively.

A major challenge in spectral decomposition is the inherent ambiguity of the solution, which is illustrated by the following relation:

$$\boldsymbol{D} \approx \boldsymbol{C}\,\boldsymbol{R}\,\boldsymbol{R}^{-1}\boldsymbol{S}^T = \boldsymbol{C}_{\text{mixed}}\boldsymbol{S}_{\text{mixed}}^T \tag{3}$$

where $\boldsymbol{R}$ is a 2×2 rotation matrix. This is commonly referred to as rotational ambiguity [28,29]. To obtain the pure (unmixed) spectral component $\boldsymbol{S}$ a reliable estimation of the coefficients for both the fluorescence and Raman components is required. The fluorescence intensity is derived from the signal in the silent region where no Raman peaks are present. However, it is difficult to reliably estimate the Raman intensity from fluorescence-dominated spectra because weak Raman peaks are easily buried by noise, which is intensified in the presence of a fluorescence background.

We incorporated prior knowledge into the estimation of Raman intensity to address the rotational ambiguity of spectral decomposition. When Raman scattering and fluorescence originate from different molecular species, photobleaching-induced molecular structural changes in the fluorescent species do not affect the Raman intensity. In addition, in the absence of photodamage, the Raman intensity remains unchanged during acquisition with a constant laser power. Accordingly, the Raman coefficient vector $\boldsymbol{c}_R$ is assumed to be constant, and all elements of $\boldsymbol{c}_R$ are set to 1. The values of $\boldsymbol{c}_F$ are estimated from the intensity in the silent region of the Raman spectra by utilizing broad fluorescence spectra in the silent region and then normalizing to their initial value to fix the relative intensity scale. Using this approach, both Raman and fluorescence spectra are estimated. This estimation is not applicable when laser irradiation or photobleaching affects the Raman signal.

Once the coefficient matrix $\boldsymbol{C}$ is determined, the desired spectral matrix $\boldsymbol{S}$ is obtained using the classical least squares (CLS) method as follows:

$$\boldsymbol{S}^T = \left(\boldsymbol{C}^T\boldsymbol{C}\right)^{-1}\boldsymbol{C}^T\boldsymbol{D} \tag{4}$$

In our method, using a single fluorescence component is a rational choice to suppress collinearity and ensure stable spectral estimation. Introducing multiple fluorescence components leads to strong collinearity, because their temporal decay profiles during photobleaching are often similar. As a result, the matrix $\boldsymbol{C}$ becomes ill-conditioned, and the inversion of $\boldsymbol{C}^T\boldsymbol{C}$ significantly amplifies noise in the CLS solution [30].

It is well known that fluorescence spectra are sensitive to the molecular state and local environment, including changes in molecular structure, intermolecular interactions, and temperature [31]. Therefore, assuming the presence of a single fluorescence component during photobleaching may lead to residual baseline components in the extracted Raman spectra. The residual baseline arising from the use of the single-fluorescence model was further reduced by applying a baseline correction. A similar baseline correction step is used in SERDS to suppress residual baseline components [3,4,6,10,32–34]. In this study, the adaptive smoothness parameter-penalized least-squares (asPLS) method [35,36] was used. Fig. 1 shows a flowchart of the proposed method.

3. Results

3.1. Proof-of-concept simulations

We validated the proposed method using simulated spectral datasets

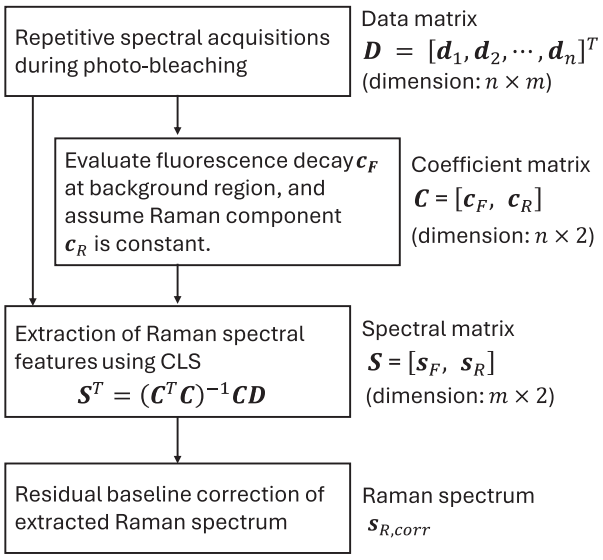

Fig. 1. Flowchart of the photobleaching-assisted spectral extraction method. The obtain matrices or vectors are written on the right side of each step. Here, n and m denote the number of acquisitions and the number of pixels in the spectral axis, respectively.

to model the photobleaching process over 1000 repeated acquisitions. The extracted Raman spectra were compared to the baseline-corrected averaged spectrum as a reference. The background variation and cosine similarity were used as metrics for peak recognition and similarity to the ground-truth Raman spectrum, respectively.

Fig. 2a shows the ground-truth Raman and fluorescence spectra. The ground-truth Raman spectrum was constructed in the range 600–1800 cm^{-1} with a wavenumber interval of 1 cm^{-1}. Lorentzian peaks with logarithmically varying intensities were placed at 200 cm^{-1} intervals, centered at 600, 800, 1000, 1200, 1400, and 1600 cm^{-1}, with intensities of 50, 10, 100, 5, 2, and 20, respectively. All peaks had a full width at half maximum (FWHM) of 20 cm^{-1}. The fluorescence spectrum was modeled as a Gaussian peak centered at 1200 cm^{-1} with an FWHM of 2000 cm^{-1} and intensity of 20,000.

The spectral coefficients obtained for 1000 acquisitions are shown in Fig. 2b. Fluorescence decay was modeled as a combination of three exponential decay components with decay rates of 1, 0.1, and 0.01 per acquisition, representing different photobleaching kinetics.

The measured spectra were generated under these conditions by incorporating instrument-derived spectral variations and stochastic noise. A 1% sinusoidal ripple with 100 cm^{-1} period and pixel-to-pixel variations with a root-mean-square intensity of 0.25% were introduced to model instrument-derived spectral variations. These values are typical of the filter ripple and sensitivity nonuniformity of CCD detectors used in Raman spectrophotometry. Subsequently, signal-dependent shot noise and readout noise with a root-mean-square intensity of 10 e^- were added. The synthesized spectra corresponding to the 1st, 10th, 100th, and 1000th acquisitions are shown in Fig. 2c.

Fig. 2d presents the Raman and fluorescence spectra obtained using the proposed method. Ground-truth Raman peaks are observed in the estimated Raman spectrum. The imposed instrument-derived spectral variations are not visible in the estimated Raman spectrum but appear in the estimated fluorescence spectrum.

The estimated fluorescence spectrum was compared to the simulated fluorescence spectrum, which included instrument-derived spectral variations (Fig. 3e). The estimated fluorescence spectrum clearly retains the imposed instrument-derived spectral variations, including both sinusoidal ripples and pixel-to-pixel sensitivity variations. The estimated fluorescence spectrum is not identical to the simulated fluorescence spectrum because of the presence of shot and readout noises.

The estimated Raman spectrum was compared with that obtained using a conventional reference. The baseline-corrected averaged spectrum, calculated using the equation below, was used as the conventional method. The ground truth fluorescence spectrum ($\boldsymbol{s}_{F,truth}$) was then subtracted from the baseline component.

$$\boldsymbol{d}_{ave,corr} = \frac{1}{n}\sum_{i}^{n}\boldsymbol{d}_i - \left(\frac{1}{n}\sum_{i}^{n}c_i\right)\boldsymbol{s}_{F,truth} \quad (5)$$

The estimated Raman spectrum and baseline-corrected averaged spectrum ($\boldsymbol{d}_{ave,corr}$) are shown in Fig. 2f. Unlike the estimated Raman spectrum, $\boldsymbol{d}_{ave,corr}$ exhibits residual instrument-derived spectral variations. We quantified background variation as the standard deviation in the 1800–2000 cm^{-1} region, where no Raman bands are present (Table 1). The background variation in the estimated Raman spectrum is comparable to that of shot noise, whereas the variation in the baseline-corrected averaged spectrum is larger. In addition, the cosine similarity to the ground-truth Raman spectrum was calculated, showing a higher similarity for the estimated Raman spectrum. These results demonstrate that the proposed method yields Raman spectra with reduced instrument-derived spectral variations, which aids spectral interpretation.

Next, we compared the suppression of the background variation under different fluorescence intensities and instrument-derived spectral variations relative to the reference conditions described above. In the latter case, we varied only the sinusoidal ripple intensity to emulate the etaloning effect. The fluorescence intensity and sinusoidal ripple intensity increased by factors of two and four, respectively, relative to the reference conditions (Fig. 3a, d). The extracted Raman spectra and baseline-corrected averaged spectra (Fig. 3b, c, e, and f) were calculated from simulated data using the procedures described above. The background variations in the silent region for each condition are summarized in Table 2.

No noticeable instrument-derived spectral variations are observed in the extracted Raman spectra, even as the fluorescence intensity and sinusoidal ripple intensity are increased (Fig. 3b, e). These results suggest that the instrument-derived spectral variations are sufficiently small relative to the shot noise level, as the variation in the silent region increases approximately in proportion to the square root of the fluorescence intensity (Table 2). In contrast, instrument-derived spectral variations are observed in the averaged spectra, and their intensities increase with fluorescence intensity and sinusoidal ripple intensity (Fig. 3c, f). The variation in the silent region increases linearly with fluorescence intensity, whereas the ripple intensity contributes an additional linear component because the pixel-to-pixel variation remains unchanged (Table 2).

3.2. Proof-of-concept experiment

Proof-of-concept experiments were conducted using fluorescent beads. Nile Red-stained polystyrene beads with a diameter of 1 μm (F8819, Invitrogen, Thermo Fisher Scientific) were used as a test sample. Polystyrene and Nile Red served as the Raman and fluorescence sources, respectively. Nile Red exhibits an absorption maximum at approximately 535 nm and a fluorescence emission peak at approximately 565 nm. The fluorescent beads were dispersed on microscope glass slides and their spectra were acquired using a confocal Raman microscope (RAMANtouch, Nanophoton) with a 532 nm excitation laser. The laser power irradiating the sample was set to 1 mW and the laser beam was focused using a 100× objective lens (numerical aperture = 0.9). A pinhole with a diameter of 50 μm (0.7 Airy units) was used as the confocal aperture. Spectral acquisition was performed continuously for 1000 consecutive frames with an exposure time of 40 ms per frame.

Fig. 4a shows the spectra measured at the 1st, 10th, 100th, and 1000th acquisitions. The fluorescence from Nile Red gradually decreases as the measurement progressed owing to photobleaching. The average

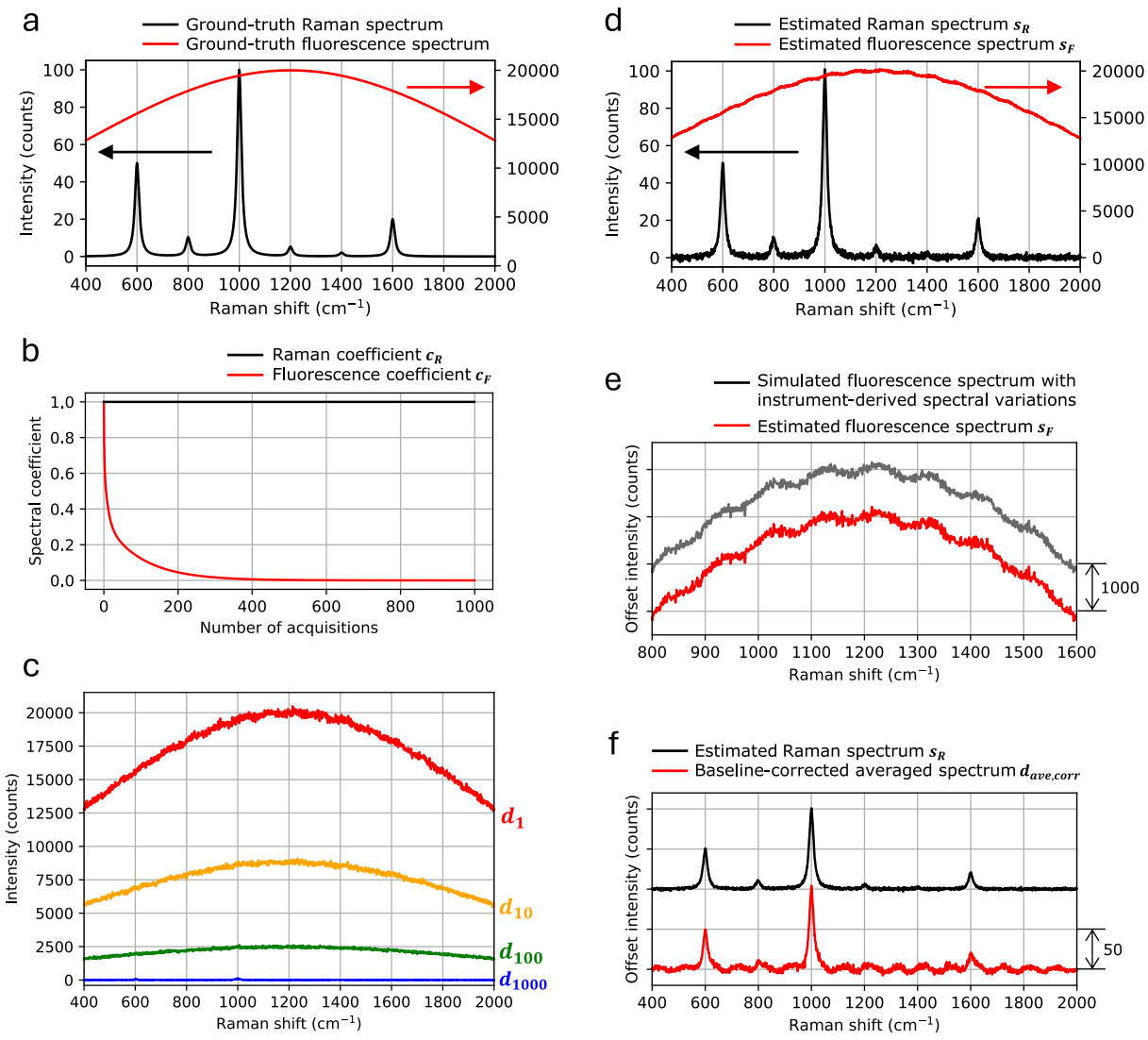

Fig. 2. (a) Defined ground-truth Raman and fluorescence spectrum. (b) Defined spectral coefficients with repeated acquisitions. (c) Spectra generated after 1, 10, 100, and 1000 acquisitions during photobleaching, including instrument-derived spectral variations (1% ripple and 0.25% pixel-to-pixel variations), shot noise, and readout noise. (d) Raman and fluorescence spectra estimated using the proposed method. (e) Comparison of the estimated and defined fluorescence spectra including instrument-derived spectral variations. (f) Comparison of the estimated Raman spectrum with the baseline-corrected averaged spectrum. In (e,f), spectra are vertically offset for clarity.

intensity in the silent region (1800–2000 cm^{-1}) was used as the fluorescence coefficient $\boldsymbol{c}_F$ (Fig. 4b).

Fig. 4c shows the spectra obtained using the proposed method. One spectrum contains more Raman signals, whereas the other mainly contains fluorescence signals. Instrument-derived spectral variations are predominantly observed in the fluorescence-rich spectrum and are negligible in the Raman-rich spectrum. Baseline fluctuations in the Raman-rich spectrum may have originated from changes in the fluorescence spectrum during the photobleaching process, leading to a mismatch with the model's assumption that the fluorescence spectrum is represented by a single component (Fig. S1). Residual baseline fluctuations can be removed using a baseline correction algorithm, because the baseline intensity and associated instrument-derived spectral variations are sufficiently small.

We compared the spectral shapes of the extracted Raman spectrum and the averaged spectrum after baseline correction with the ground-truth polystyrene Raman spectrum (Fig. 4d). The ground-truth Raman spectrum was obtained by measuring 10 μm pure polystyrene beads (01–00-104, micromod). The extracted Raman spectrum exhibits no evident instrument-derived spectral variations and its overall spectral shape is similar to that of the ground-truth spectrum. In contrast, the averaged spectrum shows instrument-derived spectral variations associated with an increasing baseline, including ripple structures and pixel-to-pixel variations. Cosine similarity results calculated excluding silent regions (1700–2700 cm^{-1} and above 3300 cm^{-1}) confirm the similarity of the extracted Raman spectrum and ground-truth spectrum, yielding values of 0.96 for the extracted Raman spectrum and 0.77 for the averaged spectrum.

The limit of detection (LOD) for peak recognition in the extracted Raman spectrum was calculated, and detectable peaks were identified based on the LOD. The LOD was defined as three times the standard deviation of the background variation (LOD = 3σ) measured in the silent region (1800–2000 cm^{-1}). The silent region close to the fingerprint region was used as a representative reference for LOD estimation, as the variation level depends on the fluorescence intensity and therefore varies with the wavenumber. Fig. 4e shows the spectra in the low-intensity region along with an estimated LOD value of 0.90. Weak peaks, indicated by the arrows in Fig. 4e,are observed in the extracted Raman spectrum but not in the baseline-corrected averaged spectrum.

Next, the reproducibility of the proposed method was evaluated. Ten

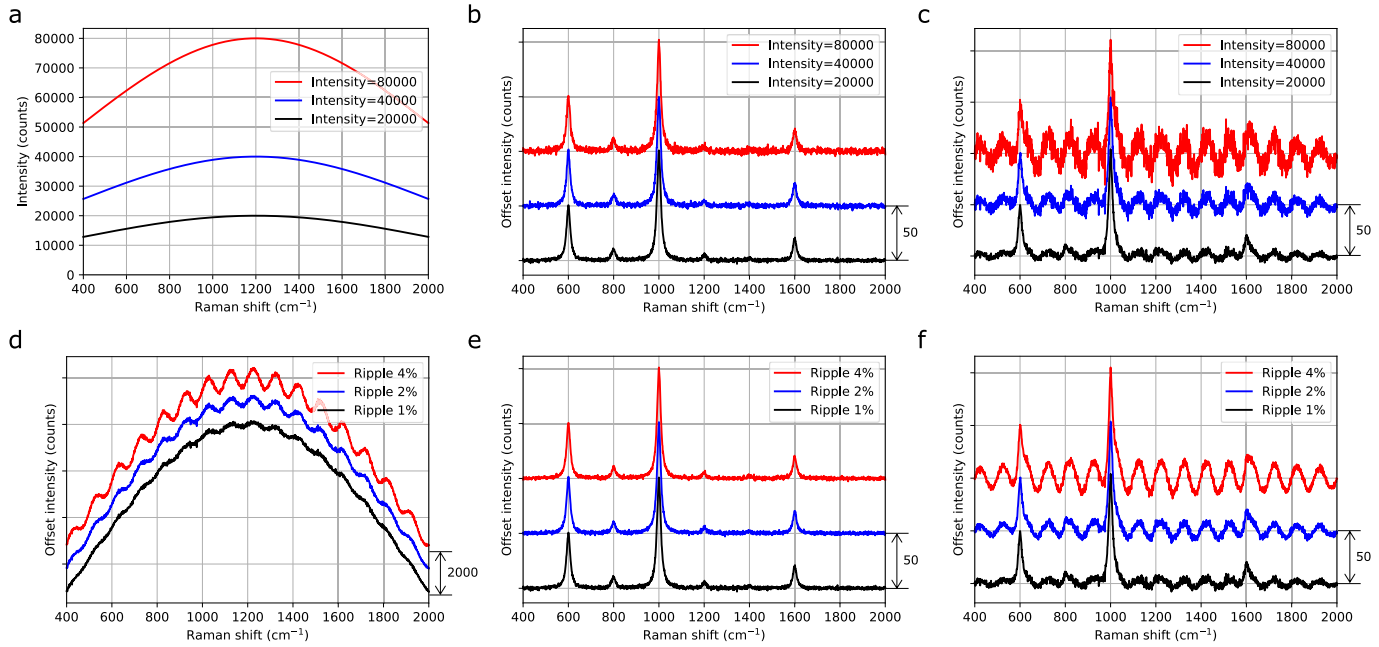

Fig. 3. Dependence of (a–c) fluorescence intensity and (d–f) sinusoidal ripple intensity on the Raman spectra. (a) Simulated fluorescence spectra with intensities of 20,000, 40000, and 80,000. (b) Extracted Raman spectra. (c) Baseline-corrected averaged spectra. (d) Simulated fluorescence spectra with sinusoidal ripple intensities of 1%, 2%, and 4%. (e) Extracted Raman spectra. (f) Baseline-corrected averaged spectra. (b–f) Spectra are vertically offset for clarity.

Table 1
Background variation (standard deviation) in the 1800–2000 cm^{-1} region and cosine similarity to the ground-truth Raman spectrum for both the estimated Raman spectrum and the baseline-corrected averaged spectrum.

Evaluated spectrum	Background variation (counts)	Cosine similarity to the ground truth
Estimated Raman spectrum	0.79	0.997
Baseline-corrected averaged spectrum	2.20	0.968

Table 2
Background variation (standard deviation) in the 1800–2000 cm^{-1} region as a function of fluorescence intensity and sinusoidal ripple intensity for both the extracted Raman spectrum and baseline-corrected averaged spectrum.

Fluorescence intensity	Sinusoidal ripple intensity (%)	Extracted Raman spectra (counts)	Baseline-corrected averaged spectra (counts)
20,000	1	0.79	2.20
40,000	1	1.10	4.41
80,000	1	1.64	8.65
20,000	2	0.79	3.94
20,000	4	0.83	7.62

independent measurements were performed using different beads under the same experimental conditions. The extracted Raman spectra consistently reproduce the characteristic Raman features of polystyrene across all measurements (Fig. 5). The cosine similarity to the ground-truth polystyrene spectrum over the ten measurements is 0.95 ± 0.0062 (mean ± standard deviation), while the background variation evaluated in the silent region (1800–2000 cm^{-1}) is 0.27 ± 0.027. These results demonstrate that the proposed method yields reproducible Raman spectra.

3.3. Application of the method to the measurement of poly(ether ether ketone)

We applied the proposed method to a fluorescent poly (ether ether ketone) (PEEK) sample. Polymeric materials are commonly analyzed using Raman spectroscopy and can exhibit strong fluorescence owing to impurities or additives.

We employed both 532 and 785 nm excitation wavelengths to verify the general applicability of the proposed method, as the photobleaching efficiency and instrument-derived spectral variations depend on the excitation wavelength. The 532 nm wavelength is widely used in commercial Raman instruments because of its strong Raman scattering efficiency, superior detection efficiency, and broad availability. However, shorter wavelengths often induce strong fluorescence. On the other hand, near-infrared excitation light in the 700–800 nm range, including 785 nm, is commonly employed to suppress fluorescence. Although fluorescence is reduced at longer wavelengths, residual fluorescence causes etaloning, an interference pattern arising from back-illuminated CCD detectors, making it difficult to obtain clean Raman spectra.

The experimental setup consisted of a Raman microscope (RAMANtouch, Nanophoton) equipped with a back-illuminated CCD detector. For 532 nm excitation, the laser power was set to 2 mW with an exposure time of 50 ms for each acquisition. For 785 nm excitation, the laser power and exposure time were set to 50 mW and 200 ms, respectively. A 20× objective lens (numerical aperture = 0.45) and a 50 μm confocal pinhole were employed for both measurements. Raman spectra were continuously measured over 10,000 acquisitions. The averaged intensity in the silent region (1750–1850 cm^{-1}) was used as the fluorescence coefficient for the decomposition of both datasets.

The spectra measured using 532 nm excitation at the 1st, 10th, 100th, 1000th, and 10000th acquisitions are shown in Fig. 6a. As the measurements progressed, the fluorescence intensity gradually decreases, but Raman peaks are barely discernible owing to the initially strong fluorescence. The proposed method successfully extracted Raman- and fluorescence-rich spectra (Fig. 6b). By isolating the instrument-derived spectral variations, particularly the pixel-to-pixel sensitivity variation, the Raman spectrum of the sample material is effectively visualized. The residual baseline variation was corrected

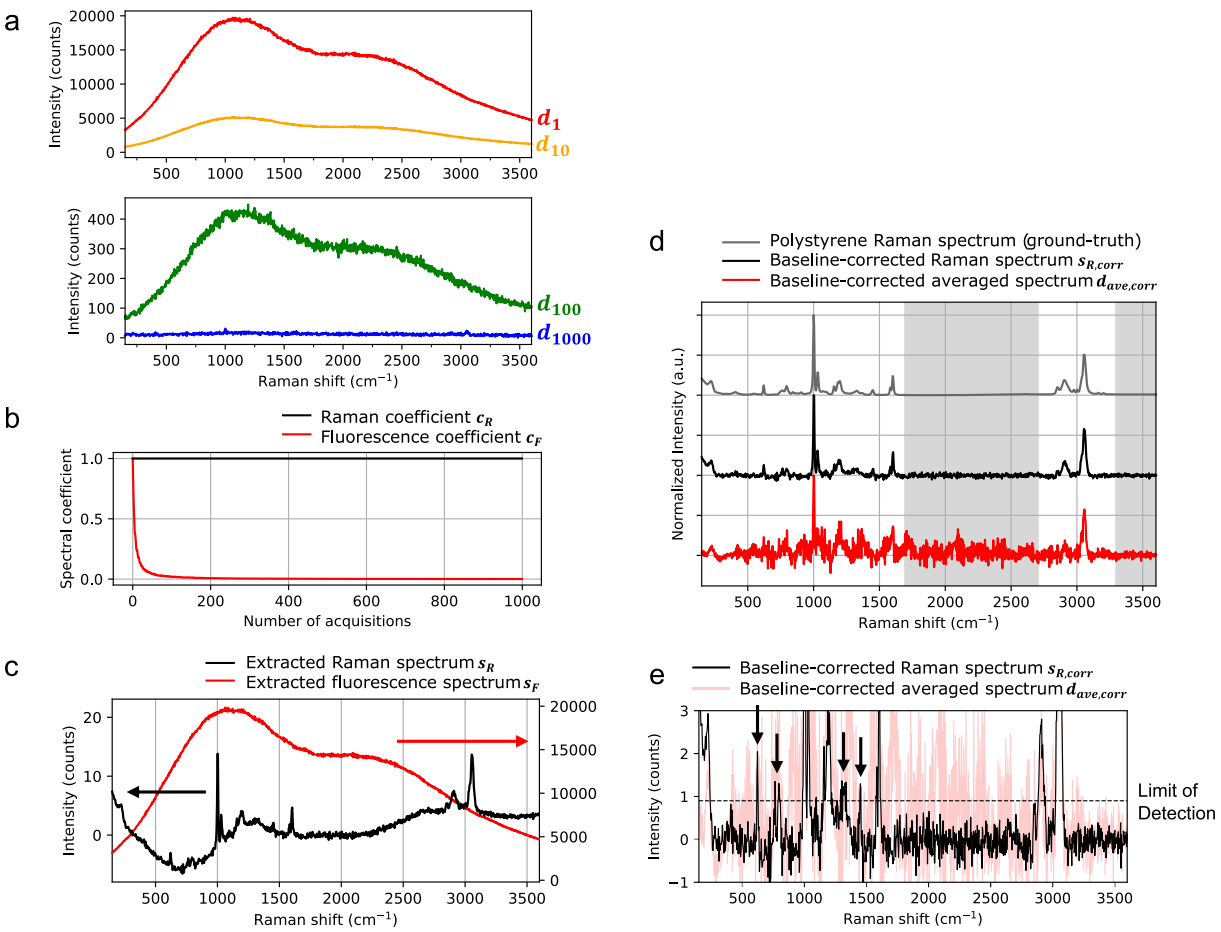

Fig. 4. (a) Measured spectra (1st, 10th, 100th, and 1000th acquisitions). (b) Spectral intensity coefficients for Raman and fluorescence spectra. (c) Extracted Raman- and fluorescence-rich spectra. (d) Spectral comparison among polystyrene (ground truth spectrum), the baseline-corrected extracted Raman spectrum, and the baseline-corrected averaged spectrum. Baseline correction was performed using the adaptive smoothness parameter penalized least-squares (asPLS) method. The smoothness parameter λ was set to 4×10^6 for the extracted Raman spectrum and 2×10^5 for the averaged spectrum. Spectra are vertically offset for clarity. (e) Enlarged view of the low-intensity region of the baseline-corrected extracted Raman spectrum and baseline-corrected averaged spectrum.

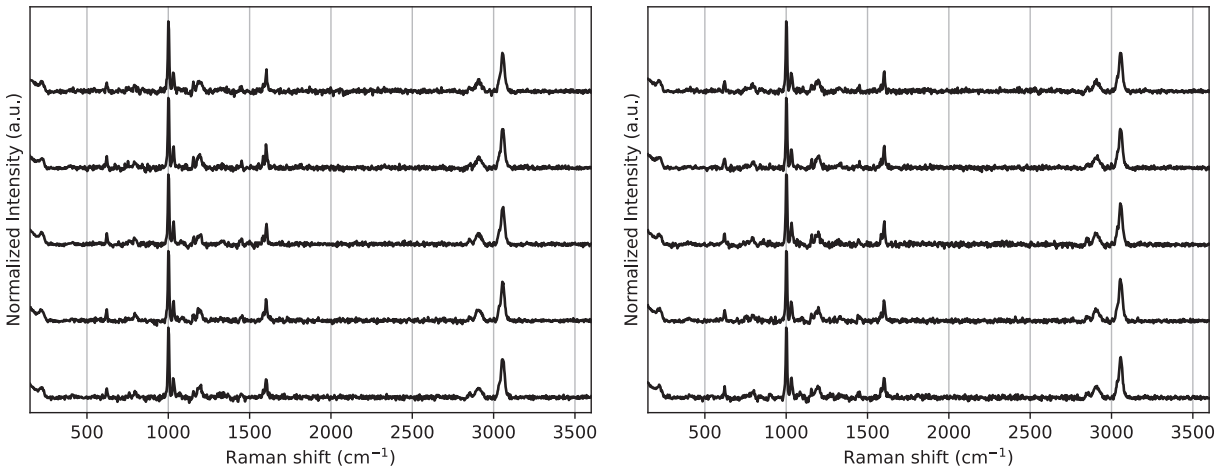

Fig. 5. Reproducibility of the extracted Raman spectra for different fluorescent bead samples. Spectra are vertically offset for clarity.

using the baseline correction method to extract the Raman spectrum (Fig. 6c). Even weak Raman peaks are visible, and the overall spectral profile shows good agreement with previously reported Fourier transform (FT)-Raman results [37,38].

The spectra measured using 785 nm excitation at the 1st, 10th, 100th, 1000th, and 10000th acquisitions are shown in Fig. 7a. The fluorescence intensity decreases over the course of the measurements due to photobleaching. The baseline exhibits periodic variations that are attributed to etaloning caused by the back-illuminated CCD detector. With 785 nm excitation, the separated spectra appropriately represent the Raman and fluorescence-rich components (Fig. 7b). Because periodic variations due to etaloning are largely captured within the

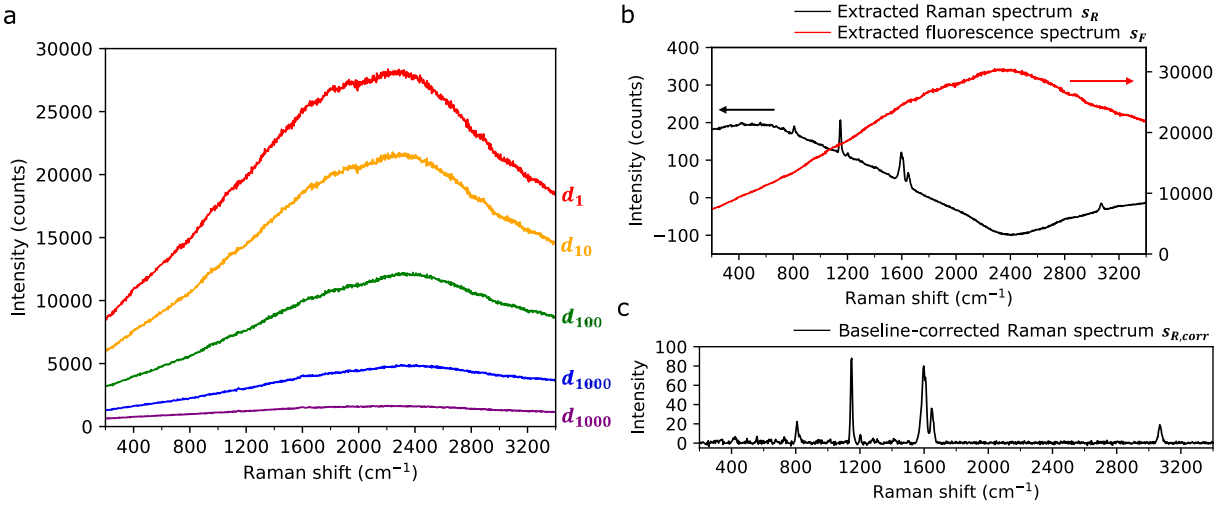

Fig. 6. (a) Spectra measured using 532 nm excitation (1st, 10th, 100th, 1000th, and 10000th acquisitions). (b) Extracted Raman- and fluorescence-rich spectra. (c) The Raman spectrum was baseline corrected using the adaptive smoothness parameter penalized least squares (asPLS) method with a smoothness parameter $\lambda = 10^5$.

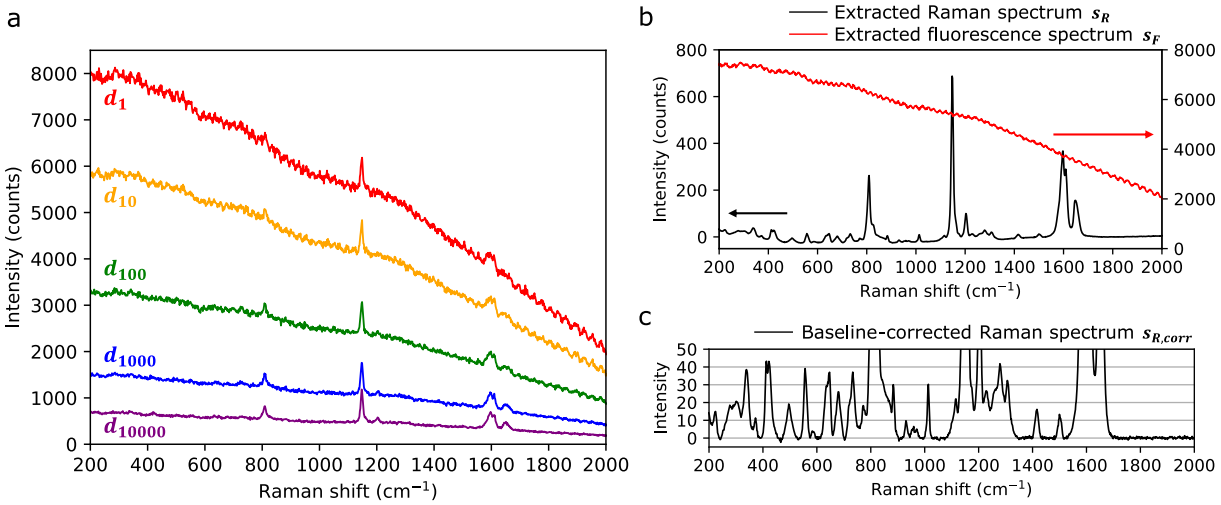

Fig. 7. (a) Spectra measured using 785 nm excitation at the 1st, 10th, 100th, 1000th, and 10000th acquisitions. (b) Extracted Raman and fluorescence spectra. (c) Raman spectrum baseline corrected using the adaptive smoothness parameter penalized least squares (asPLS) method with a smoothness parameter $\lambda = 10^7$.

fluorescence component, a clear Raman spectrum is obtained without instrument-derived spectral variations, particularly those arising from

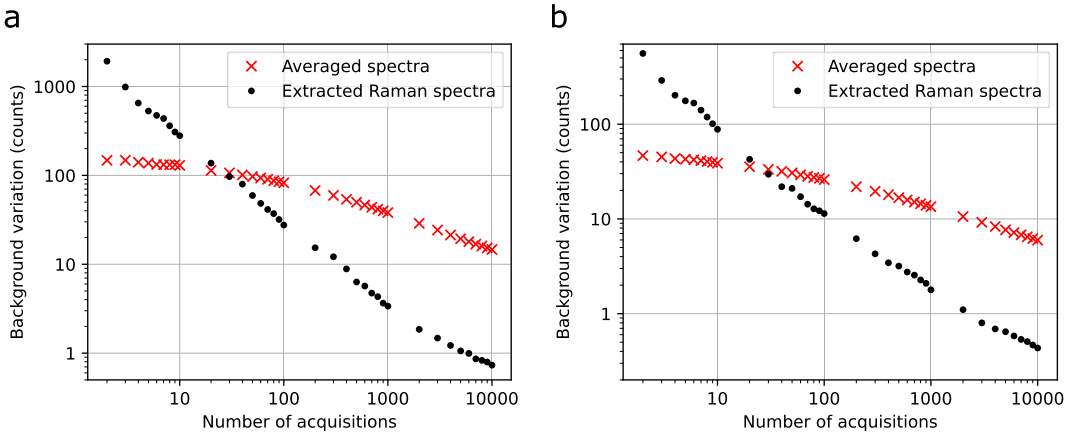

Fig. 8. Background variation as a function of the number of acquisitions for (a) 532 nm and (b) 785 nm excitation wavelengths. The variation was calculated as the standard deviation in the 1750–1850 cm^{-1} region after baseline correction using the adaptive smoothness parameter penalized least squares (asPLS) method ($\lambda = 10^5$ for 532 nm excitation, and $\lambda = 10^7$ for 785 nm excitation).

the etaloning effect. Weak peaks with intensities below 10 counts are clearly visible (Fig. 7c). This spectrum also shows good agreement with previously reported FT-Raman spectra [37,38].

The residual baseline fluctuations observed using 785 nm excitation are smaller than those obtained under 532 nm excitation. This is probably because multiple fluorescent species contribute under 532 nm excitation, whereas fluorescence under 785 nm excitation may be dominated by a single fluorescent species, which is consistent with the single-component assumption in the model.

Since the proposed method relies on photobleaching and its performance evolves over repeated acquisitions, we evaluated the relationship between the background variation and number of acquisitions for both the extracted Raman spectrum and averaged spectrum. The background variation was calculated in the silent region from 1750 to 1850 cm^{-1}. Both spectra were baseline-corrected before evaluation. As shown in Fig. 8, for both excitation wavelengths, the averaged spectrum exhibits a lower variation level in the early stages of measurement, even though it contains instrument-derived spectral variations. As photobleaching progresses with continued acquisition, the extracted Raman spectrum shows lower variation. For the present dataset, the crossover between the variation levels in the extracted and averaged spectra occurs after approximately 30 acquisitions in both cases, beyond which the proposed method consistently outperforms the averaged spectrum. Therefore, this crossover point serves as an indicator of which spectrum is preferable under certain conditions. As the number of acquisitions increases, the difference in background variation between the two methods continues to widen, eventually reaching 20.0-fold and 13.6-fold improvements for the 532 and 785 nm excitation wavelengths, respectively. The magnitude of these improvements depends on several factors, including the signal-to-background ratio (SBR), instrument-derived spectral variations, photobleaching rate, and stability of the fluorescence and Raman spectra during acquisition.

4. Discussion

The proposed method extracts Raman spectra without requiring prior information. Such as instrument-derived spectral variations, and is based on a linear model in which the spectral shape is preserved. Although changes in the fluorescence spectrum during photobleaching can introduce a residual baseline in the extracted Raman spectrum, instrument-derived background variation can be reduced compared to the unprocessed spectrum. This baseline can be corrected because it is generally much broader than the Raman bands, and instrument-derived spectral variations have already been reduced.

The proposed method does not remove stochastic noise components, and it should be noted that the influence of shot noise cannot be eliminated. If instrument-derived spectral variations are perfectly removed through prior calibration, the SNR of the baseline-corrected averaged spectrum will be comparable to that obtained using the proposed method. Nevertheless, the accurate calibration of instrument-derived spectral variations is difficult and labor-intensive because the variations depend on many factors, including the sample type, measurement conditions, and instrument alignment. Therefore, the proposed method, similar to SERDS, suppresses instrument-derived spectral variations by canceling them under identical sample and measurement conditions, thereby providing a practical approach for removing instrument-derived spectral variations without prior calibration.

However, the proposed method has several limitations. First, it is difficult to apply the method when the observed Raman spectra change during measurement; for example, due to sample motion, bleaching of specific Raman bands under resonance conditions [39,40], photodamage, or the formation of byproducts under laser irradiation [41,42]. These laser-induced effects are more likely when visible excitation leads to absorption or when shorter excitation wavelengths with higher photon energies are used. Therefore, longer excitation wavelengths are generally more suitable for applying the proposed method.

Second, this method is difficult to apply when measuring fluorescent molecules. Photobleaching can alter the molecular structure, leading to changes in the Raman spectral profile, such as variations in the overall spectral intensity, peak width, peak position, and relative peak intensity. Furthermore, the validity of the obtained Raman spectra should be carefully verified when photobleaching causes chemical or structural modification of a sample, as may occur in biological specimens, or when chemically unstable molecules undergo secondary reactions during irradiation. However, it has been reported that the use of photobleaching does not cause significant changes in the Raman spectrum of dyes [24], and isalso applicable for biological samples such as bone [19] and skin [20]. Therefore, this method may be applicable to such samples.

Third, the presence of multiple fluorescent species or changes in the fluorescence spectrum during photobleaching can lead to residual baseline components and instrument-derived spectral variations in the extracted Raman spectra. Artifacts introduced by baseline correction are usually not obvious; however, the algorithm and parameters must be carefully chosen to minimize distortion of the Raman spectrum.

Regarding spectral changes during photobleaching, fluorescence spectra can exhibit shifts in peak positions and changes in bandwidth due to various factors, such as the molecular state or local environment [31]. This suggests that the excitation wavelengths closer to the emission peak are more likely to induce spectral changes during photobleaching. Therefore, depending on the sample, selecting an excitation wavelength that avoids the fluorescence emission peak may mitigate changes in the fluorescence spectral shape, which could improve the consistency with the assumptions of the model used in this study.

When applying this approach to practical polymer measurements, such as the fluorescent PEEK sample described above, sufficient photobleaching is required for reliable extraction (Fig. S2). Because achieving sufficient photobleaching often requires time, this method may not be suitable for dynamic measurements or when the sample changes over time. During long measurements, practical issues may arise, such as fluctuations in the laser power or wavelength, focus drift on the sample, and variations in the spectrometer or other optical components, all of which can introduce errors.

Several methods can be used to accelerate photobleaching. First, the removal of out-of-focus signals is effective. For example, using a confocal setup and increasing the degree of confocality, i.e., employing a higher-NA objective or a smaller confocal pinhole [43,44] and targeting a smaller specimen volume [45], have been reported to enhance photobleaching. Secondly, increasing the excitation power can further accelerate photobleaching [19,20,24,45]. However, caution is required because heat accumulation during prolonged measurements can damage the sample.

In the experiments using the PEEK sample and 785 nm excitation (Fig. 7), the dataset was measured up to 10,000 times to illustrate the improvement in the background variation as a function of the number of acquisitions, resulting in a long total acquisition time. However, in practical applications, the measurement can be terminated once a sufficient SNR has been achieved. The required SNR depends on the evaluation objective (material identification, evaluation of peak positions or widths, or analysis of intensity ratios) and the desired level of accuracy.

The proposed method offers advantages over conventional numerical methods, such as polynomial fitting [46–48], asymmetric least squares [35,49,50], and extended multiplicative signal correction [51] because they treat the baseline as a smooth component and therefore cannot remove instrument-derived spectral variations. Although slowly varying oscillatory patterns can be suppressed, such suppression often introduces artifacts, including the removal of low-frequency spectral components. To improve the SNR, filtering methods such as Gaussian smoothing, Fourier-domain filtering, and wavelet-based denoising often suppress high-frequency components. Consequently, both the noise and high-frequency components of the Raman peaks can be attenuated, which can lead to peak broadening and related artifacts.

Similar to the proposed method, SERDS removes instrument-derived spectral variations originating from fluorescence background. This method can be implemented relatively easily by modifying only the excitation source. Compared with the proposed method, SERDS is less dependent on the sample type; however, it requires the excitation wavelength shift the be adjusted according to the spectral resolution and Raman peak linewidth. In addition, spectral reconstruction from difference spectra can introduce distortions in the Raman band shapes, particularly for overlapping bands or those with varyingwidths [4,32]. The SNR of the reconstructed spectrum is also degraded by subtraction [32]. Another limitation of SERDS is that the fluorescence level must remain the same between spectra measured at different excitation wavelengths. In contrast to the proposed method, photobleaching can lead to residual fluorescence and instrument-derived spectral variation in SERDS measurements [6,32,34,52,53]. Several practical strategies have been used to avoid this problem, such as performing alternating measurements while rapidly switching the excitation wavelength [6,52,53] or pre-photobleaching the sample before the measurement to stabilize the fluorescence level.

Another effective approach for suppressing fluorescence in Raman measurements is time-resolved Raman spectroscopy [54,55]. In this technique, sub-nanosecond laser pulses are used, and temporal gating is applied to detect only signals within time windows with a high SBR. Unlike the proposed method and SERDS, time-resolved Raman spectroscopy suppresses fluorescence detection itself, thereby reducing instrument-derived spectral variations and the shot noise of the fluorescence background. Recently, short-term gating has become easier to implement using single-photon avalanche diode detectors [55].

The proposed method can be applied to time-resolved Raman spectroscopy data. Spectra acquired with sequential time windows provide data with different Raman and fluorescence intensities. The resulting contrast in intensity changes reduces the collinearity of the temporal profiles, making the data suitable for decomposition using a least-squares method. Therefore, this combination can potentially enable a more reliable extraction of Raman spectral features in time-resolved Raman spectroscopy.

5. Conclusions

The proposed method enables the extraction of Raman spectral features based on a linear model, in which the spectral shape is preserved during exposure. Both simulations and experiments demonstrated that the method is particularly effective in the presence of large instrument-derived spectral variations (e.g., etaloning).

The prerequisite conditions of the method are that the shapes of both the observed Raman and fluorescence spectra remain largely unchanged during measurement and that their spectral coefficients can be estimated from the measurement conditions or the measured data. Regarding spectral stability, longer excitation wavelengths are generally more suitable for applying this method.

The novelty of the proposed method is its simplicity and practicality. It requires no hardware modifications or additional optical components and relies only on repeated acquisitions. Data processing is straightforward and based on classical least squares analysis. Furthermore, the method is compatible with typical commercial confocal Raman systems.

The improvement in Raman peak recognition achieved by removing instrument-derived spectral variations is consistent with the effect observed in SERDS. In SERDS, the subtraction of the spectra measured at slightly shifted excitation wavelengths effectively eliminates the background and instrument-derived spectral variations, thereby enabling the extraction of clear Raman spectra. In our method, the Raman signal remains constant, while the fluorescence varies along the intensity axis, whereas in SERDS, the fluorescence remains constant and only the Raman peaks shift along the wavenumber axis. Although the components and axes of variation differ between the two methods, both reconstruct Raman spectra by removing the background and instrument-derived spectral variations from measured fluorescence-containing spectra.

However, the proposed method has several limitations, including enhanced background variations under conditions of insufficient photobleaching and the presence of multiple fluorescence components. In future work, we aim to address these issues and further improve estimation accuracy.

Supplementary data to this article can be found online at https://doi.org/10.1016/j.saa.2026.127926.

Declaration of competing interest

The authors declare the following financial interests/personal relationships which may be considered as potential competing interests: Yusuke Shiozaki reports financial support and equipment were provided by Bruker Japan K.K. Yusuke Shiozaki reports a relationship with Bruker Japan K.K. that includes: employment, equity or stocks, and travel reimbursement. Yusuke Shiozaki has patent pending to Bruker Japan K. K. If there are other authors, they declare that they have no known competing financial interests or personal relationships that could have appeared to influence the work reported in this paper.

Acknowledgments

This work was partially supported by the Japan Science and Technology Agency (JST) under Grant Number JPMJPF2009 (COI-NEXT).

Data availability

Data will be made available on request.

References

[1] B.T. Bowie, D.B. Chase, I.R. Lewis, P.R. Griffiths, Anomalies and artifacts in Raman spectroscopy, in: J.M. Chalmers, P.R. Griffiths (Eds.), Handb. Vib. Spectrosc., 1st ed.Wiley, 2001, https://doi.org/10.1002/0470027320.s3103.
[2] J.M. Smulko, N.C. Dingari, J.S. Soares, I. Barman, Anatomy of noise in quantitative biological raman spectroscopy, Bioanalysis 6 (2014) 411–421, https://doi.org/10.4155/bio.13.337.
[3] A.P. Shreve, N.J. Cherepy, R.A. Mathies, Effective rejection of fluorescence interference in raman spectroscopy using a shifted excitation difference technique, Appl. Spectrosc. 46 (1992) 707–711.
[4] J. Zhao, M.M. Carrabba, F.S. Allen, Automated fluorescence rejection using shifted excitation raman difference spectroscopy, Appl. Spectrosc. 56 (2002) 834–845.
[5] J.B. Cooper, M. Abdelkader, K.L. Wise, Sequentially shifted excitation raman spectroscopy: novel algorithm and instrumentation for fluorescence-free raman spectroscopy in spectral space, Appl. Spectrosc. 67 (2013) 973–984, https://doi.org/10.1366/12-06852.
[6] F. Korinth, T.A. Shaik, J. Popp, C. Krafft, Assessment of shifted excitation raman difference spectroscopy in highly fluorescent biological samples, Analyst 146 (2021) 6760–6767, https://doi.org/10.1039/D1AN01376A.
[7] C. Xie, Y. Li, Confocal micro-Raman spectroscopy of single biological cells using optical trapping and shifted excitation difference techniques, J. Appl. Phys. 93 (2003) 2982–2986, https://doi.org/10.1063/1.1542654.
[8] M. Maiwald, G. Erbert, A. Klehr, H.-D. Kronfeldt, H. Schmidt, B. Sumpf, G. Tränkle, Rapid shifted excitation raman difference spectroscopy with a distributed feedback diode laser emitting at 785 nm, Appl. Phys. B Lasers Opt. 85 (2006) 509–512, https://doi.org/10.1007/s00340-006-2459-8.
[9] M.A. da S. Martins, D.G. Ribeiro, E.A.P. dos Santos, A.A. Martin, A. Fontes, H. da S. Martinho, Shifted-excitation raman difference spectroscopy for in vitro and in vivo biological samples analysis, Biomed. Opt. Express 1 (2010) 617–626, https://doi.org/10.1364/BOE.1.000617.
[10] M.T. Gebrekidan, C. Knipfer, F. Stelzle, J. Popp, S. Will, A. Braeuer, A shifted-excitation raman difference spectroscopy (SERDS) evaluation strategy for the efficient isolation of raman spectra from extreme fluorescence interference, J. Raman Spectrosc. 47 (2016) 198–209, https://doi.org/10.1002/jrs.4775.
[11] M. Maiwald, B. Sumpf, G. Tränkle, Rapid and adjustable shifted excitation raman difference spectroscopy using a dual-wavelength diode laser at 785 nm, J. Raman Spectrosc. 49 (2018) 1765–1775, https://doi.org/10.1002/jrs.5456.
[12] L.S. Theurer, M. Maiwald, B. Sumpf, Shifted excitation raman difference spectroscopy: a promising tool for the investigation of soil, Eur. J. Soil Sci. 72 (2021) 120–124, https://doi.org/10.1111/ejss.12928.
[13] K. Sowoidnich, M. Oster, K. Wimmers, M. Maiwald, B. Sumpf, Shifted excitation raman difference spectroscopy as enabling technique for the analysis of animal feedstuff, J. Raman Spectrosc. 52 (2021) 1418–1427, https://doi.org/10.1002/jrs.6140.

[14] K. Sowoidnich, M. Maiwald, M. Ostermann, B. Sumpf, Shifted excitation raman difference spectroscopy for soil component identification and soil carbonate determination in the presence of strong fluorescence interference, J. Raman Spectrosc. 54 (2023) 1327–1340, https://doi.org/10.1002/jrs.6500.
[15] T.R. Gilson, P.J. Hendra, Laser Raman Spectroscopy, Wiley-Interscience, 1970.
[16] H.J. Sloane, R. Bramston-Cook, Raman spectroscopy of some polymers and copolymers of styrene, butadiene, and methylmethacrylate, Appl. Spectrosc. 27 (1973) 217–225.
[17] S. Higuchi, J. Tanaka, S. Tanaka, Experimental investigation on determination of trace amounts of some colored compounds by resonance raman spectrometry, J. Spectrosc. Soc. Jpn. 27 (1978) 353–359, https://doi.org/10.5111/bunkou.27.353.
[18] D.L.A. de Faria, M.A. de Souza, Raman spectra of human skin and nail excited in the visible region, J. Raman Spectrosc. 30 (1999) 169–171, https://doi.org/10.1002/(SICI)1097-4555(199903)30:3<169::AID-JRS365>3.0.CO;2-P.
[19] K. Golcuk, G.S. Mandair, A.F. Callender, N. Sahar, D.H. Kohn, M.D. Morris, Is photobleaching necessary for raman imaging of bone tissue using a green laser? Biochim. Biophys. Acta Biomembr. 1758 (2006) 868–873, https://doi.org/10.1016/j.bbamem.2006.02.022.
[20] M.E. Darvin, N.N. Brandt, J. Lademann, Photobleaching as a method of increasing the accuracy in measuring carotenoid concentration in human skin by raman spectroscopy, Opt. Spectrosc. 109 (2010) 205–210, https://doi.org/10.1134/S0030400X10080096.
[21] A.M. Macdonald, P. Wyeth, On the use of photobleaching to reduce fluorescence background in raman spectroscopy to improve the reliability of pigment identification on painted textiles, J. Raman Spectrosc. 37 (2006) 830–835, https://doi.org/10.1002/jrs.1510.
[22] F. Bonnier, S.M. Ali, P. Knief, H. Lambkin, K. Flynn, V. McDonagh, C. Healy, T. C. Lee, F.M. Lyng, H.J. Byrne, Analysis of human skin tissue by raman microspectroscopy: dealing with the background, Vib. Spectrosc. 61 (2012) 124–132, https://doi.org/10.1016/j.vibspec.2012.03.009.
[23] H. Wang, J. Zhao, A.M.D. Lee, H. Lui, H. Zeng, Improving skin raman spectral quality by fluorescence photobleaching, Photodiagnosis Photodyn. Ther. 9 (2012) 299–302, https://doi.org/10.1016/j.pdpdt.2012.02.001.
[24] J. Zięba-Palus, A. Michalska, Photobleaching as a useful technique in reducing of fluorescence in raman spectra of blue automobile paint samples, Vib. Spectrosc. 74 (2014) 6–12, https://doi.org/10.1016/j.vibspec.2014.06.007.
[25] M. Tatarkovič, A. Synytsya, L. Šťovíčková, B. Bunganič, M. Miškovičová, L. Petruželka, V. Setnička, The minimizing of fluorescence background in raman optical activity and raman spectra of human blood plasma, Anal. Bioanal. Chem. 407 (2015) 1335–1342, https://doi.org/10.1007/s00216-014-8358-7.
[26] S.B. Dutta, H. Krishna, K.M. Khan, S. Gupta, S.K. Majumder, Fluorescence photobleaching of urine for improved signal to noise ratio of the raman signal – an exploratory study, Spectrochim. Acta A Mol. Biomol. Spectrosc. 247 (2021) 119144, https://doi.org/10.1016/j.saa.2020.119144.
[27] W.H. Lawton, E.A. Sylvestre, Self modeling curve resolution, Technometrics 13 (1971) 617–633, https://doi.org/10.1080/00401706.1971.10488823.
[28] J.-H. Jiang, Y. Ozaki, Self-modeling curve resolution (smcr): principles, techniques, and applications, Appl. Spectrosc. Rev. 37 (2002) 321–345, https://doi.org/10.1081/ASR-120014359.
[29] R. Tauler, A. Smilde, B. Kowalski, Selectivity, local rank, three-way data analysis and ambiguity in multivariate curve resolution, J. Chemometr. 9 (1995) 31–58, https://doi.org/10.1002/cem.1180090105.
[30] Detecting and Assessing Collinearity, in: Regres. Diagn., John Wiley & Sons, Ltd, 1980, pp. 85–191, https://doi.org/10.1002/0471725153.ch3.
[31] J.R. Lakowicz, Principles of Fluorescence Spectroscopy, Springer US, Boston, MA, 1999, https://doi.org/10.1007/978-1-4757-3061-6.
[32] E. Cordero, F. Korinth, C. Stiebing, C. Krafft, I.W. Schie, J. Popp, Evaluation of shifted excitation raman difference spectroscopy and comparison to computational background correction methods applied to biochemical raman spectra, Sensors 17 (2017), https://doi.org/10.3390/s17081724.
[33] M.T. Gebrekidan, R. Erber, A. Hartmann, P.A. Fasching, J. Emons, M. W. Beckmann, A. Braeuer, Breast tumor analysis using shifted-excitation raman difference spectroscopy (SERDS), Technol. Cancer Res. Treat. 17 (2018) 1533033818782532, https://doi.org/10.1177/1533033818782532.
[34] S. Yerolatsitis, A. Kufcsák, K. Ehrlich, H.A.C. Wood, S. Fernandes, T. Quinn, V. Young, I. Young, K. Hamilton, A.R. Akram, R.R. Thomson, K. Finlayson, K. Dhaliwal, J.M. Stone, Sub millimetre flexible fibre probe for background and fluorescence free raman spectroscopy, J. Biophotonics 14 (2021) e202000488, https://doi.org/10.1002/jbio.202000488.
[35] F. Zhang, X. Tang, A. Tong, B. Wang, J. Wang, Y. Lv, C. Tang, J. Wang, Baseline correction for infrared spectra using adaptive smoothness parameter penalized least squares method, Spectrosc. Lett. 53 (2020) 222–233, https://doi.org/10.1080/00387010.2020.1730908.
[36] D. Erb, pybaselines: A Python library of algorithms for the baseline correction of experimental data, 2024, https://doi.org/10.5281/ZENODO.5608581.
[37] J.K. Agbenyega, G. Ellis, P.J. Hendra, W.F. Maddams, C. Passingham, H.A. Willis, J. Chalmers, Applications of fourier transform raman spectroscopy in the synthetic polymer field, spectrochim, Acta part Mol. Spectrosc 46 (1990) 197–216, https://doi.org/10.1016/0584-8539(90)80090-L.
[38] G. Ellis, M. Naffakh, C. Marco, P.J. Hendra, Fourier transform raman spectroscopy in the study of technological polymers part 1: poly(aryl ether ketones), their composites and blends, spectrochim, Acta. a. Mol. Biomol. Spectrosc 53 (1997) 2279–2294, https://doi.org/10.1016/S1386-1425(97)00168-6.
[39] C. Onogi, H. Hamaguchi, Photobleaching of the "raman spectroscopic signature of life" and mitochondrial activity in rho− budding yeast cells, J. Phys. Chem. B 113 (2009) 10942–10945, https://doi.org/10.1021/jp903478r.
[40] K.A. Okotrub, N.V. Surovtsev, Photobleaching of the resonance raman lines of cytochromes in living yeast cells, J. Photochem. Photobiol. B 141 (2014) 269–274, https://doi.org/10.1016/j.jphotobiol.2014.10.008.
[41] G.J. Puppels, J.H.F. Olminkhof, G.M.J. Segers-Nolten, C. Otto, F.F.M. de Mul, J. Greve, Laser irradiation and raman spectroscopy of single living cells and chromosomes: sample degradation occurs with 514.5 nm but not with 660 nm laser light, Exp. Cell Res. 195 (1991) 361–367, https://doi.org/10.1016/0014-4827(91)90385-8.
[42] Y. Kumamoto, A. Taguchi, N.I. Smith, S. Kawata, Deep UV resonant raman spectroscopy for photodamage characterization in cells, Biomed. Opt. Express 2 (2011) 927, https://doi.org/10.1364/BOE.2.000927.
[43] R. Tabaksblat, R.J. Meier, B.J. Kip, Confocal raman microspectroscopy: theory and application to thin polymer samples, Appl. Spectrosc. 46 (1992) 60–68, https://doi.org/10.1366/0003702924444434.
[44] N. Gierlinger, T. Keplinger, M. Harrington, Imaging of plant cell walls by confocal raman microscopy, Nat. Protoc. 7 (2012) 1694–1708, https://doi.org/10.1038/nprot.2012.092.
[45] D. Seo, D. Lim, J. Seo, D. Shin, Quantification of auto-photobleaching effects during raman measurements for microplastic detection, Sens. Actuators B Chem. 423 (2025) 136702, https://doi.org/10.1016/j.snb.2024.136702.
[46] C.A. Lieber, A. Mahadevan-Jansen, Automated method for subtraction of fluorescence from biological raman spectra, Appl. Spectrosc. 57 (2003) 1363–1367.
[47] F. Gan, G. Ruan, J. Mo, Baseline correction by improved iterative polynomial fitting with automatic threshold, Chemom, Intel. Lab. Syst. 82 (2006) 59–65, https://doi.org/10.1016/j.chemolab.2005.08.009.
[48] J. Zhao, H. Lui, D.I. McLean, H. Zeng, Automated autofluorescence background subtraction algorithm for biomedical raman spectroscopy, Appl. Spectrosc. 61 (2007) 1225–1232.
[49] P.H.C. Eilers, A perfect smoother, Anal. Chem. 75 (2003) 3631–3636, https://doi.org/10.1021/ac034173t.
[50] Z.-M. Zhang, S. Chen, Y.-Z. Liang, Baseline correction using adaptive iteratively reweighted penalized least squares, Analyst 135 (2010) 1138–1146, https://doi.org/10.1039/B922045C.
[51] H. Martens, E. Stark, Extended multiplicative signal correction and spectral interference subtraction: new preprocessing methods for near infrared spectroscopy, J. Pharm. Biomed. Anal. 9 (1991) 625–635, https://doi.org/10.1016/0731-7085(91)80188-F.
[52] K. Sowoidnich, M. Towrie, M. Maiwald, B. Sumpf, P. Matousek, Shifted excitation raman difference spectroscopy with charge-shifting charge-coupled device (CCD) lock-in detection, Appl. Spectrosc. 73 (2019) 1265–1276.
[53] F. Korinth, E. Schmälzlin, C. Stiebing, T. Urrutia, G. Micheva, C. Sandin, A. Müller, M. Maiwald, B. Sumpf, C. Krafft, G. Tränkle, M.M. Roth, J. Popp, Wide field spectral imaging with shifted excitation raman difference spectroscopy using the nod and shuffle technique, Sensors 20 (2020) 6723, https://doi.org/10.3390/s20236723.
[54] R.P. Van Duyne, D.L. Jeanmaire, D.F. Shriver, Mode-locked laser raman spectroscopy. New technique for the rejection of interfering background luminescence signals, Anal. Chem. 46 (1974) 213–222, https://doi.org/10.1021/ac60338a012.
[55] M. Kögler, B. Heilala, Time-gated raman spectroscopy – a review, Meas. Sci. Technol. 32 (2020) 012002, https://doi.org/10.1088/1361-6501/abb044.